

Mg-Modified Zn-Co-Fe-La Nano Ferrites: A Study of Structural, Morphological, Vibrational, Electro-Optical, Dielectric and Magnetic Evolution

M. I. Arshad^{1,2,3*}, M. S. Hasan^{4**}, Atta Ur Rehman³, N. Amin³, Le Duc Tung¹, Nguyen Thi Kim Thanh^{1,2***}, N. A. Morley⁵, Mongi Amami⁶, Faisal Alresheedi⁷, Safa Ezzine⁶, M. A. Gadhi⁸

¹*Biophysics Group, Department of Physics and Astronomy, University College London, Gower Street, London, WC1E 6BT, UK.*

²*UCL Healthcare Biomagnetic and Nanomaterials Laboratories, 21 Albemarle Street, London W1S 4BS, UK*

³*Department of Physics, Govt. College University Faisalabad, 38000, Pakistan.*

⁴*Department of Physics, The University of Lahore, Lahore 53700, Pakistan*

⁵*Department of Materials Science and Engineering, The University of Sheffield, S1 3JD, UK*

⁶*Department of Chemistry, College of Sciences, King Khalid University, Abha 61412, Saudi Arabia*

⁷*Department of Physics, College of Science, Qassim University, Buraidah 51452, Saudi Arabia*

⁸*Bahawalpur Institute of Nuclear Medicine and Oncology (BINO) Bahawalpur, Pakistan*

Corresponding authors email: *miarshadgcuf@gmail.com, **m.sajjadhasan@hotmail.com, ***ntk.thanh@ucl.ac.uk

Abstract

The series of $Zn_{0.4}Co_{0.6-x}Mg_xFe_{1.9}La_{0.1}O_4$ ($x = 0.0, 0.15, 0.30, 0.45, 0.6$) nanoferrites prepared via co-precipitation technique. Scherrer and Williamson-Hall (W-H) methods were used to find the crystallite size (29.6-39.2 nm and 31.6-36.3 nm, respectively) and lattice constant was calculated (8.4063-8.3954 Å). Moreover, Fourier transform infrared (FTIR) spectroscopy revealed the existence of absorption bands along with functional groups. The vibrations of O^{2-} ions at the tetrahedral and octahedral sites were shown by the Raman five active modes. DC resistivity reduced in the range of $5.2961 \times 10^8 \Omega \text{ cm}$ to $9.6453 \times 10^7 \Omega \text{ cm}$ for $x = 0.0$ to $x = 0.6$, respectively. The maximum DC resistivity and activation energy (0.1035 eV) were obtained at the parent sample ($Zn_{0.4}Co_{0.6}Fe_{1.9}La_{0.1}O_4$). The optical bandgaps reduced from 2.61

to 1.47 eV, as the Mg^{2+} contents increased. With increasing frequency the dielectric loss and the dielectric constant decrease. The magnetic parameters such as saturation magnetization ($M_s = 60.82-25.94$ emu/g), remnant magnetization ($M_r = 47.82-18.64$ emu/g), and coercivity ($H_c = 1334-511$ Oe) demonstrated reducing trends with the increase of Mg^{2+} doping. The best magnetic behavior of the as-prepared samples suitable in microwave devices was observed for $Zn_{0.4}Co_{0.6}Fe_{1.9}La_{0.1}O_4$ sample.

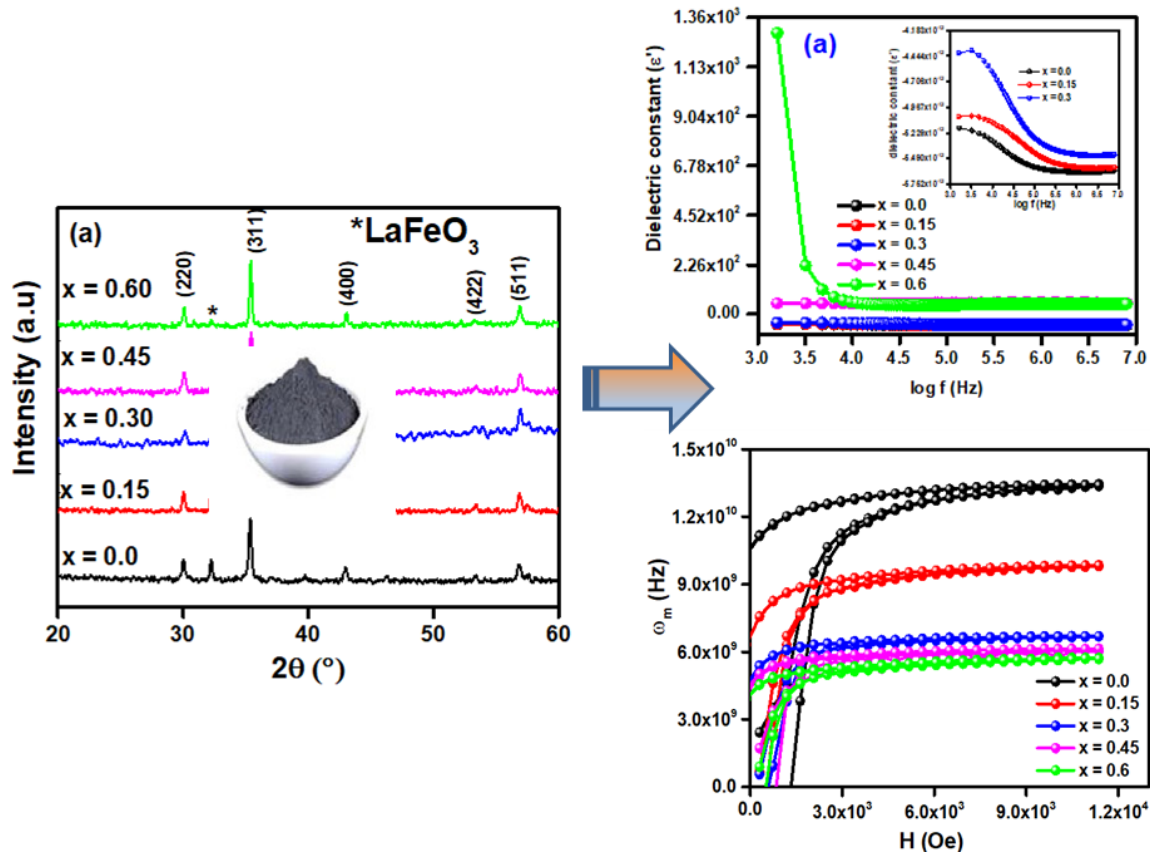
Research highlights

- $Zn_{0.4}Co_{0.6-x}Mg_xFe_{1.9}La_{0.1}O_4$ nanoferrite powder prepared by co-precipitation route
- Crystallite size was minimum at $x = 0.3$.
- The optical band gap energy decreased in the range of 2.61 – 1.47 eV
- DC resistivity also reduced from $5.2961 \times 10^8 \Omega \text{ cm}$ to $9.6453 \times 10^7 \Omega \text{ cm}$
- Based on magnetic properties the sample $Zn_{0.4}Co_{0.6}Fe_{1.9}La_{0.1}O_4$ is suitable in microwave devices

Keywords: Co-precipitation; Optical bandgap; DC resistivity; Dielectric constant; saturation magnetization.

Graphical Abstract

The maximum saturation magnetization (M_s), remnant magnetization (M_r), and coercivity (H_c) observed at $x = 0.0$ (parent sample). The peak distances and slight peak height for the nanoferrites are suggested by field dependence of the dM/dH curve at 300 K and are due to the presence of large liable superparamagnetic domains.



1 Introduction

The spinel ferrites are applicable in numerous fields due to their different properties. Nano-sized ferrite particles often exhibit unique and size-dependent properties compared to their bulk counterparts. These properties can include enhanced magnetic properties, improved electrical conductivity, and altered optical properties. Nano ferrites offer an opportunity for fundamental research to explore the effects of quantum confinement, surface interactions, and size-induced phenomena on material properties. Investigation of size effects is of scientific interest and this research contributes to our understanding of materials at the nanoscale. Nano-sized ferrites can undergo changes in crystal structure or lattice parameters, affecting their magnetic and electrical behavior. The high surface area in nano ferrites can lead to increased surface energy, which can influence the material's reactivity, stability, and surface magnetic properties. Nano-sized ferrite particles sometimes exhibit higher magnetization values compared to their bulk counterparts due to a higher surface-to-volume ratio and reduced magnetic domain size. Coercivity, which is the resistance of a material to demagnetization, can be enhanced in

nano ferrites, making them useful for applications like high-density magnetic recording. Such characteristics of spinel nano ferrites are associated to preparation route and processing conditions for magnetic stability, well and homogenous size and the shape of the nano ferrite [1]. AB_2O_4 is the universal formula for spinel ferrites where A is divalent cations, and B trivalent cations [2]. Spinel ferrite demonstrates high resistivity, low eddy current losses and high permeability [3]. By controlling the size and shape of nano ferrite particles, we can tailor their properties to meet specific application requirements. Such characteristics of spinel ferrites lead to be applicable in different fields including biomedicine [4], magnetic resonance imaging (MRI) [5], memory storage gadgets [6], microwave absorbance [7], antenna rods [8], microwave devices [9], drug delivery [10], and power transformers [11].

Different synthesis techniques including spray pyrolysis [12], the hydrothermal technique [13], refluxing microwave method [14], the self-igniting process [15, 16] and the co-precipitation route [17, 18] were used to synthesize the nano ferrite powder. Co-precipitation process is simple and economical for preparation of nanoparticles as compared to others [18]. Co-precipitation can be conducted using environmentally friendly reagents and conditions, aligning with principles of green chemistry, which promote sustainable and eco-friendly practices in chemical processes. Moreover, this synthesis method offers benefits in terms of regulating particle size, achieving molecular homogeneity, and facilitating swift reactions [19-21].

Thomas *et al.*, prepared the Mg^{2+} inserted Co^{2+} soft ferrites by the application of solution combustion process. The maximum crystallite size (D) was 113 nm at $x = 0.2$. Saturation magnetization ($56-34 \text{ emug}^{-1}$) and coercivity (930-89 Oe) were reduced with the increment of Mg^{2+} [16]. Mammo *et al.*, determined the effects of Mg^{2+} inserted Co^{2+} nano-ferrites fabricated by sol-gel auto combustion process. The DC resistivity increased up to $10^7 \Omega.cm$ and saturation magnetization decreased with Mg^{2+} doping and recommended the nano-particles for higher-frequency electronic devices [15]. Bhukal *et al.*, synthesized the Mg-doped Zn–Co nano composites by sol-gel auto combustion procedure and observed the electrical resistivity up to $10^9 \Omega.cm$. With the increase of Mg^{2+} insertion the saturation magnetization decreased from 55.13 to 24.17 emu/g [22]. Lodhi *et al.*, developed the $MgCo_xZn_{1-x}Fe_2O_4$ soft ferrites by employing a micro-emulsion route and stated the reduction in crystallite size and lattice constant with the addition of magnesium. The optimized magnetic properties of sample with $x=0.5$ suggests the use in high-density recording media [23]. Rafiq *et al.*, prepared Mg–Zn nanocrystals with Co^{2+}

doping by co-precipitation route and found that the lattice constant decreased with doping of Co^{2+} . The minimum coercivity was observed at $x = 0.15$ [24]. Liu *et al.*, synthesized the $\text{Ni}_{0.5}\text{Zn}_{0.4}\text{Mg}_{0.1}\text{La}_{0.1}\text{Fe}_{1.99}\text{O}_4$ nano ferrite by self-igniting process and reported the grain size of 26 nm. The as-prepared materials were annealed at 1023 K and suggested that Mg-La doped Ni-Zn sample applicable in electromagnetic wave attenuation [25]. Gaba *et al.* studied the physical properties of $\text{MgLa}_x\text{Fe}_{2-x}\text{O}_4$ ferrites for microwave absorption applications. The extreme coercivity ($H_c = 30.59$ Oe) and saturation magnetization ($M_S = 19.39$ emug⁻¹) were noticed at $x = 0.05$ [26]. Thomas Dippong *et al.* synthesized the SiO_2 inserted Co ferrites and found the reduction in crystallite size with the addition of silica matrix [27]. They also observed the effect of Co/Fe ratio on oxide nanoparticles and found the crystallite size less than 100 nm [19]. Paul Barvinschi *et al.* prepared the cobalt ferrite- SiO_2 nanocomposites and found the crystallite size in the range of 3 to 10 nm [28]. Thomas Dippong *et al.* investigated the sonophotocatalytic activity SiO_2 embedded Mn-Zn ferrites [29].

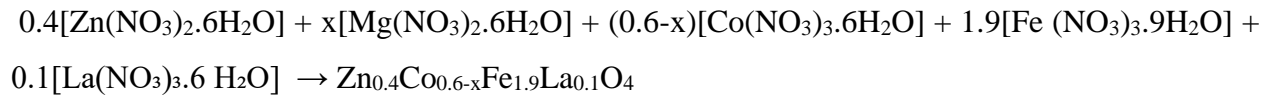
This research investigates how the introduction of magnesium ions affects the structural, morphological, vibrational, electro-optical, dielectric, and magnetic properties of these ferrites. Notably, the material exhibits decreased resistivity, reduced optical band gap energy and magnetization. These findings suggest improved conductivity and reduced microwave absorption, making it promising for efficient microwave device applications, such as waveguides and antennas. This research contributes to advancing microwave technology by harnessing the unique characteristics of Mg-modified ferrites.

In our work, the Mg^{2+} doped ZCL nano ferrites with compositional formula $\text{Zn}_{0.4}\text{Co}_{0.6-x}\text{Mg}_x\text{Fe}_{1.9}\text{La}_{0.1}\text{O}_4$ ($x = 0.0, 0.15, 0.3, 0.45, 0.6$) were developed by co-precipitation procedure. Here, Zn-Co-La nano ferrite was chosen from among numerous spinel ferrites due to its tailored properties, potential for enhanced performance, and existing research literature highlighting its effectiveness in similar applications. Its availability, research gap-filling potential, and specific advantages in niche areas also played a role in this selection, aligning with the research objectives and making it a practical and promising candidate for the study. The ZCL nanoferrites are specially synthesized for their microwave applications. The structural, morphological, vibrational, electro-optical, dielectric and magnetic characteristics of nano ferrite samples were determined.

2 Experimental

2.1 Synthesis Process

Mg²⁺ substituted Zn_{0.4}Co_{0.6-x}Fe_{1.9}La_{0.1}O₄ ($x = 0.0, 0.15, 0.3, 0.45, 0.6$) powder were prepared by co-precipitation process. 99.9% pure Sigma-Aldrich salts including zinc nitrate [Zn(NO₃)₂.6H₂O], magnesium nitrate [Mg(NO₃)₂.6 H₂O], cobalt nitrate [Co(NO₃)₂.6H₂O], iron nitrate [Fe (NO₃)₃.9H₂O] and lanthanum nitrate [La(NO₃)₃.6 H₂O] were used. The weights given in [Table 1](#), with the help of Ja1003c 0.001g Internal Calibration Digital Electronic Analytical Balance of Zn, Mg, Co, Fe and La nitrates were inserted in deionized water according to the stoichiometric ratios. At 60 °C, the solutions were mixed with continuous stirring (78-I magnetic stirrer). NaOH solution was inserted as a precipitous factor to retain pH 12. The following chemical reaction appeared for the formation of nanoferrites:



They were kept in 80 °C pre-heated water (Kambic water bath) for 12 hrs. To remove impurities from precipitates the solutions were cleaned with deionized water and ethanol by the support of filter papers. Then the particles were dried in an oven (Biotechnologies inc. oven) at 80 °C. The obtained materials were grind into powder by using granite mortar pestle. The obtained samples were sintered (DM-12N Dming Technology Muffle furnace) at 800 °C for 4 hrs and 10 min and following the grounding for fine powder. The schematic diagram of preparation powder is given in [Fig. 1](#).

2.2 Characterization Techniques

The spinel cubic structures in nanoferrite samples were confirmed by X-ray Diffraction (Bruker D8) where Cu-K_α is source with $\lambda = 1.5406 \text{ \AA}$. Morphology of nano-ferrites was studied with Scanning Electron Microscopy (SEM). Two probes I-V system with Keithley 2401 was employed to investigate electrical properties. Ultraviolet-visible (UV-vis) photometer was utilized to study the optical bandgap energy. FTIR spectroscopy (Perkin) was used to investigate the absorption bands within the 400–3500 cm⁻¹ frequency range. Raman spectroscopy was applied to determine vibrational properties. Dielectric parameters were investigated through LCR meter. Vibrating Sample Magnetometer (VSM) was employed to study the magnetic nature of fabricated nanocomposites with the application of magnetic field up to 1.5 T.

3 Results and Discussions

3.1 Structural study

X-ray diffractograms for of Mg^{2+} doped ZCL nanoferrites are presented in Fig. 2 (a-b). The prominent peaks specified with (220), (311), (400), (422), and (511) confirmed the spinel structure of as-prepared nano ferrites (space group; $F d-3 m$) [30] and peak marked with symbol (*) belongs to orthorhombic configuration LaFeO_3 (space group; $P b n m$) [31, 32]. Volume of LaFeO_3 was decreased with the substitution of Mg^{2+} . It can be seen from Fig. 2 (b) peak (311) shifts towards larger angle up to $x = 0.3$ and for $x = 0.45$ to 0.6 towards smaller angle. The shift towards smaller angles for $x = 0.45$ to 0.6 implies a decrease in lattice spacing. This suggests that as the concentration of Mg^{2+} ions increases in this range, their smaller ionic radius draws neighboring atoms closer together, resulting in a reduction of the crystal lattice spacing. The observed peak shifts are a result of changes in the crystal lattice's atomic arrangement caused by the substitution of Mg^{2+} ions, with the direction of the shift depending on the ionic radius of Mg^{2+} and its concentration in the material.

The Bragg's angle for peak (311) and d-spacing (d) calculated using Bragg's law [33] are reported in Table 2. For crystallite size (D), Scherrer's formula was applied [34]. The crystallite size has lowest value of 24.88 nm at $x = 0.3$ (Table 2). Mg^{2+} ions have a smaller ionic radius compared to Co^{2+} ions. When Mg^{2+} ions are substituted for Co^{2+} ions in the crystal lattice, the smaller size of Mg^{2+} ions allows them to occupy the lattice sites more closely together. This leads to a more compact crystal structure with smaller crystallites. The increase in particle aggregation with higher magnesium ion content in the prepared samples can be attributed to the smaller ionic radius of magnesium ions compared to the host ions in the material. When magnesium ions are introduced in greater quantities, they can occupy spaces within the crystal lattice that would normally be filled by larger host ions. This disrupts the regular crystal structure, leading to increased particle aggregation as the lattice becomes more compact. Essentially, the smaller magnesium ions create a tighter packing of particles, resulting in larger aggregations within the material. Previously, M. S. Hasan *et al.* found the crystallite size showing the similar trend for Mg and La co-doped ferrites [17]. Scherrer formula only describes the consequence of crystallite size on broadening of peaks and do not enlighten the production of straining during crystal evolution because of point effect and grain boundary. In order to explain this factor Williamson-Hall (W-H) method is applied which states that the peak broadening is

addition of size and strain. So, $\beta = \beta_{\text{size}} + \beta_{\text{strain}}$. Therefore, $\beta = \frac{0.9\lambda}{D} \times \frac{1}{\cos\theta} + 4\epsilon \tan\theta$. On rearranging the equation, we get; $\beta \cos\theta = \epsilon (4\sin\theta) + \frac{0.9\lambda}{D}$. Fig.3 is the W-H plots with $4\sin\theta$ versus $\beta \cos\theta$ indicating the XRD peak for Mg^{2+} substituted ZCL nanoferrites. The average crystallite is determined by straight line interception and lattice strain created during crystal growth is calculated by slope. In the crystal matrix the strain is based on lattice narrowing or extension corresponding to size than bulk [35]. Table 2 illustrates the average crystallite obtained through W-H plot. 23.81 nm ($x = 0.3$) is the lowest calculated average crystallite size value obtained from W-H method as illustrated in Table 2. Furthermore, the lattice strain showed maximum value for $x = 0.3$ obtained from W-H plot.

The experimental lattice constant (a_{exp}) [36] was calculated and reported in Table 2. It can be seen that, for $x = 0.3$, the experimental lattice constant (a_{exp}) was minimum. The dissimilarities in lattice constants are associated to the difference in ionic radii of Mg^{2+} (0.72 Å) and Co^{2+} (0.74 Å) and peak shifts with the dopant concentration (Fig. 2(b)). The introduction of Mg^{2+} ions disrupts the regular crystal lattice, causing lattice distortion. This distortion can result in smaller crystallites as it becomes energetically favorable for the crystal to form smaller domains with fewer lattice defects. Also, the decrease in lattice constant with an increase in Mg concentration and a decrease in Co concentration can be explained by the fact that Mg ions have a smaller ionic radius compared to Co ions. This difference in ionic radii leads to a closer packing of ions in the crystal lattice, reducing the overall size of the unit cell and resulting in a smaller lattice constant. The true value of experimental lattice constant (a_0) determined by using Nelson Riley Function $F(\theta)$ plots (Fig. 4) for each reflection constructing a linear regression. In Fig. 4, we extrapolate linear line to $F(\theta) = 0$ or 90° . The calculated true values experimental lattice constant (a_0) from the y-intercept of extrapolation function $F(\theta)$ are reported in Table 2. The volume of unit cell ($V = a^3$) [37] has a minimum at $x = 0.3$. The X-ray and bulk densities (d_x and d_B) [38] were (listed in Table 2). The fact that the values of d_x are larger than those of d_B is due to the uncommon empty spaces occurrence through the preparation and annealing in nano ferrites [39]. Furthermore, d_x and d_B decreased with Mg^{2+} doping (Table 2) and the relative density percentage ($d_R = d_x/d_B$) [40] increases from 132.53 to 133.41 % for $x = 0.0$ to 0.3 and then reduced for $x = 0.45$ to 0.6. The porosity percentage [39] was determined and it has extreme result at $x = 0.3$. Different factors were calculated, like specific surface area (S) [41] and

the packing factor (p) [39]. The values for “ S ” enhance up to $x = 0.3$ with the addition of Mg^{2+} cations and then decrease. It was observed in Table 2 that the factor “ p ” has a lowest outcomes of 98.43 at $x = 0.3$. The dissimilarities in the cationic radii of Mg^{2+} and Co^{2+} cations is responsible of such behavior.

Hopping distances/lengths L_A and L_B for sub-lattice sites tetrahedral (A) and octahedral (B) between magnetic ions may cause the conductivity to increase. Table 2 showed the decrease in hopping length upto $x = 0.3$ and a small energy is essential to transfer charges amongst the cationic sites. The variation in hopping length may be due to differences in the radii of Mg^{2+} and Co^{2+} [42]. The polaron radius (γ_p) can also verify it. The values of the polaron radius (γ_p) for Mg^{2+} doped ZCL soft ferrites are given in Table 2. Reduction in the polaron radius reveals that a smaller energy is vital to transport charge carries between the cationic sites, and enhancement in values mean larger energy is needed for this purpose [43].

Tetrahedral (A) ionic radii (r_A) and octahedral (B) ionic radii (r_B) depend on cations distribution. Zn^{2+} occupies the tetrahedral A -site with normal spinel structure [44]. Co^{2+} , Mg^{2+} and Fe^{3+} cations reside both A and B sites [45, 46]. Below equations are applied to investigate ionic radii r_A and r_B for tetrahedral and octahedral sites and most suitable cations distributions are demonstrated in Table 3.

$$r_A = [C_{AZn} \cdot r(Zn^{2+}) + C_{ACo} \cdot r(Co^{2+}) + C_{AMg} \cdot r(Mg^{2+}) + C_{AFe} \cdot r(Fe^{3+})]$$

$$r_B = \frac{1}{2} [C_{BCo} \cdot r(Co^{2+}) + C_{BMg} \cdot r(Mg^{2+}) + C_{BFe} \cdot r(Fe^{3+}) + C_{BLa} \cdot r(La^{3+})] O_4$$

In above relations C and r are fractional concentrations and ionic radii respectively Zn^{2+} (0.74 \AA), Co^{2+} (0.74 \AA), Mg^{2+} (0.72 \AA), Fe^{3+} (0.64 \AA) and La^{3+} (1.06 \AA), respectively. C_{AZn} , C_{ACo} , C_{AMg} and C_{AFe} are associated to A -site concentrations and C_{BCo} , C_{BMg} , C_{BFe} and C_{BLa} B -site concentrations. Table 4 showed the ionic radii of Mg^{2+} inserted Zn-Co-La nanoferrites. It can be observed that r_A is amplified, and r_B decreases with the increase of Mg^{2+} doping for $x = 0.0 - 0.6$. The expansion in r_A is due to greater ionic radius of Co^{2+} (0.74 \AA) contents that are substituted by lower ionic radius Mg^{2+} (0.72 \AA). The reduction in r_B with the Mg^{2+} doping is because of shifting of Fe^{3+} (0.64 \AA) from B -site to A -site. From the r_A and r_B , the theoretical lattice constant (a_{th}) [39] was found and listed in Table 4. The slight difference amongst “ a_{th} ” and “ a_{exp} ” is due to variations in ionic radii, the normal arrangements of ions supposition in unit cell structure for theoretical calculations [47].

Tetrahedral sites are diminutive to provide accommodation with the metal ions and slightly shift the oxygen ions. Such shifting of O²⁻ ions is expressed as an oxygen positional parameter (U) and $U = 0.375 \text{ \AA}$ for ideal spinel structure [39]. The calculated U of fabricated spinel ferrites deviates from the standard value. Displacing of anions from ideal situation lead to deformations in sublattices and caused the deviation in U [48]. The increasing trend of U with the rising contents of Mg²⁺ may be attributed to the growth in tetrahedral sub-lattice arrangements to accommodate smaller ionic radii Mg²⁺ in replacement of larger ionic radii Co²⁺. The tolerance factor [$T = \frac{1}{\sqrt{3}} \left(\frac{r_A + R_o}{r_B + R_o} \right) + \frac{1}{\sqrt{2}} \left(\frac{R_o}{r_A + R_o} \right)$] was used to make sure that synthesized nanoparticles are free of defects as given in Table 4. For ideal ferrite structure, T is equal to unity [49]. The enhancement in measured values of T is approaching unity and stretches the nanoferrites free of contaminations. “ T ” is approximately approached to 1 for all fabricated nanoferrites and it is improved with the increasing Mg²⁺ cations.

Shortest distance at A -site cations and O²⁻ ions and B site cations and O²⁻ ions are called bond length (R_A) and (R_B), respectively [39]. Values of R_A and R_B are listed in Table 5 where inconstant trends are seen with the addition of Mg²⁺ ions. The Mg²⁺ (0.72 Å) ions shifted a large number of Fe³⁺ ions from the A to B site. Therefore, the values “ r_A ” of the A -site increase leading to an increase in tetrahedral bond length (R_A).

The inter-atomic lengths *i.e.*, tetrahedral, shared octahedral, and unshared octahedral edge lengths are represented by d_{AL} , d_{BL} , and d_{BLU} , respectively. Distinctions in bond positions d_{AL} , d_{BL} , and d_{BLU} are linked to the allocation of metal ions in A and B lattice sites and are listed in Table 5. The expansion in ionic radii of r_A with the increasing concentration of Mg²⁺ is responsible for an increase in d_{AL} . On the other hand, a decrease in d_{BL} and d_{BLU} is because of contractions in ionic radii of r_B with the increase of Mg²⁺ contents [50].

Magnetic characteristics of soft-ferrites are associated to exchange forces as well as on the inter-ionic distance and bond angles between ions. $A-B$, $A-A$ and $B-B$ are the magnetic interactions associated to bond distance and angles between the ions. The bond angles and inter-ionic distances are directly and inversely proportional to strength of magnetic exchange forces [51]. The calculated inter-ionic lengths *i.e.*, cations–anions (Me–O) and cations–cations (Me–Me) are given in Table 6. By the application of interionic distance, the bond angles were also

computed [52]. Table 7 confirmed that by enhancing the Mg^{2+} concentration, the bond angles θ_1 , θ_2 , and θ_5 decreased and signified the weak (A–B) and (A–A) interactions. The increased in θ_2 and θ_4 bond angles confirmed the strong (B–B) interaction with insertion of Mg^{2+} [50].

3.2 Morphological study

Micro images obtained from Scanning electron microscopy (SEM) are given in Fig. 5 (a-e). The micrographs (Fig.5 (a-e)) reveal that the nanoparticles have irregular shape. The accurate particle size is difficult to determine from micro images due to boundaries of particles being not clear. The observed agglomerated shapes are due to the loose packing of particles [26] and the agglomeration increases with Mg^{2+} doping. The sizes of agglomeration are in the order of few nanometers and being shown in Fig. 5 (a-e). The different size of particles may be due to presence of some impurities. Similar shapes and agglomeration of nanoparticles were determined by Mohd. Hashim *et al.* for Co doped Mg-Zn ferrites [1].

3.3 FTIR Study

Fig. 6 shows recorded FTIR spectra for Mg^{2+} doped ZCL within the frequency range from 400 to 3500 cm^{-1} . Two significant absorption bands [53], including high (γ_1) 550.96 cm^{-1} – 552.39 cm^{-1} and low (γ_2) 413.57 cm^{-1} – 403.56 cm^{-1} , are observed in this spectrum (Table 8) where, γ_1 and γ_2 are associated to tetrahedral and octahedral [54] complexes of metal oxide in the spinel matrix [47]. Previously, Santosh Bhukal *et al.* determined the low frequency band in the range of 434 cm^{-1} for Mg substituted CoZn ferrites [22]. Within ZCL ferrite samples, we observed a nearly equal distribution of Fe^{3+} ions occupying both the tetrahedral A-site and the octahedral B-site, and this distribution extends to Mg^{2+} ions as well. This implies that both electrons and holes become available at the B-site due to the coexistence of Mg^{2+} and Fe^{3+} ions. Additionally, there is an inclination for La^{3+} ions to substitute Fe^{3+} ions within the octahedral B-sites. This behavior can be rationalized by considering variations in lattice constant values corresponding to different dopant ratios or by proposing their incorporation at interstitial sites within the structural framework [26]. Besides two major absorption peaks, additional peaks at different wavenumbers also observed. Absorption band around 840 cm^{-1} can be attributed to C-C, 2356 cm^{-1} to CO_2 and OH stretching vibrations [55, 56]. Absorption peaks at 1109 cm^{-1} , 1360 cm^{-1} , and 1556 cm^{-1} are due to C-H, NO_3 group, and C=O antisymmetric stretching vibrations, respectively.

3.4 Raman Spectroscopy Study

Fig. 7 shows recorded Raman spectra for Mg²⁺ doped Zn-Co-La nano ferrites. The group theory predict five active phonon Raman modes such as; $\Gamma = 1A_{1g} + 1E_g + 3T_{2g}$ for regular spinel structure of soft ferrites [57]. The presence of an inversion center in the Centro-symmetrical space group $Fd -3m$ for similar vibrational modes, indicates the shared exclusion of Raman (R) and Infrared (IR) activities. A_{1g} (R), E_g (R), and $3T_{2g}$ (R) [58] are the five first active modes observed in the Raman spectrum at room temperature. The indication A, E, T, and g signified single, double and triple-dimension depiction and regularity to center of inversion, correspondingly [59, 60]. In the Raman analysis, a distinct peak associated with the orthorhombic configuration of LaFeO₃ was not particularly prominent. However, there were minor peaks detected within the 550-750 cm⁻¹ range, which were attributed to the presence of LaFeO₃ [61].

Following is the explanation based on the quasi-molecular depictions of soft ferrites which is associated to the regular mode movements of the tetrahedron (FeO₄): The A_{1g} (1) is attributed to Fe-O tetrahedral bonds stretching vibrations [38] appeared at 636.75-668.36 cm⁻¹, E_g and T_{2g} (3), existing in the ranges of 327.11-395.89 cm⁻¹ and 472.23-530.45 cm⁻¹ are assigned to symmetric and asymmetric bending of oxygen relative to Fe, respectively. T_{2g} (2) is associated to asymmetric stretching of Fe-O bond at 388.15-479.39 cm⁻¹ and T_{2g} (1) translational movement of entire FeO₄ at 236.19-335.29 cm⁻¹ as seen in Table 9. Same kinds of stretching vibrations were observed by M. I. Arshad *et al.* [62]. The Raman spectra of Mg²⁺ substituted ferrites and five Raman active modes revealed in Fig. 7. The existence of different parameters in crystal structure like lattice deformation, the dislocation and contaminations are responsible for the observed vibrational band modes. Apart from the XRD results showing a single-phase nano ferrites, the occurrence of the peaks in Raman spectra can be illustrated as additional assurance of crystal field distortions. In the crystal field because of the transformations in polarizability in the course of molecular vibration, the Raman active modes appear and depend upon failure of symmetry and Raman modes [60, 63].

3.5 Electrical Study

Fig. 8 (a-b) shows the plots of electrical resistivity ($\log \rho$) versus temperature (T) and the inverse of temperature ($10^3/T$). Fig. 8(a) indicates the relationship between the log of resistivity and temperature. The plots are divided into two ferromagnetic and paramagnetic region. It can be seen that resistivity of as-prepared samples increases with increasing temperature up to transition

Curie (T_c) temperature. The results indicate the semiconductor behavior of Mg^{2+} doped ZCL. Except from the hopping of electrons amongst the cations of similar elements with the valency greater than 1 distributed over the lattice site describe the conduction process in soft nano ferrites instead of energy band theory [64]. Same kind of results for resistivity of were also determined by M. S. Hasan *et al.* [17]. The Curie temperature (T_c) reduces with Mg^{2+} doping (Table 10). Fig. 8(b) demonstrates the Arrhenius plots from which the activation energy (ΔE , [$\rho = \rho_0 e^{\frac{\Delta E}{k_B T}}$]) is calculated. The ΔE of paramagnetic (E_p) is higher than the ferromagnetic region (E_f). It is because paramagnetic are disordered states, while ferromagnetic are ordered states [65]. In paramagnetic states, charge carriers need enormous energy to move compared to those in the ferromagnetic states. Activation energies ($\Delta E = E_p - E_f$) decreased with dopant concentration (Fig. 9(b)), and the outcomes are reported in Table 10. Fig. 9(a) represents the relationship amongst the ferromagnetic and paramagnetic region and resistivity decreases with the increase of Mg^{2+} doping. DC resistivity is inversely associated to drift mobility (μ_d) [66]. Fig. 10 shows drift mobility (μ_d) versus temperature. The values for “ μ_d ” increased with increasing temperature. This fact implies that the “ μ_d ” of charge carriers (thermally generated) enhances with increased temperature (T). It can be observed (Fig. 9(b)) that μ_d increases with dopant and the values of 323 K are given in Table 10.

3.6 UV-vis Spectroscopy Study

The optical bandgap energy (E_g) of nano-ferrites usually associated to grain size, impurities, lattice strain, lattice parameters, surfacial contact, and the concentration of dopant ions [67]. Fig. 11 shows Tauc plots [68] by employing the UV-vis photometer. The “ E_g ” was determined and its values are plotted in Fig. 11. The “ E_g ” reduces from 2.61 eV to 1.47 eV, as the concentration of Mg^{2+} increased. When nanoparticle structures are formed due to changes in composition, quantum confinement effects can occur. Smaller particle sizes can result in quantization of energy levels which can lead to a lower band gap of ZCL ferrites. It can be observed that optical band gap energy decreases significantly with the addition of Mg^{2+} concentration due to the quantum confinement effect [69]. The other E'_g values are also appearing in the inner sides of the Tauc’s plots for $x = 0.0-0.6$ as shown in Fig. 11 and associated results are 2.89 eV, 2.64 eV, 2.34 eV, 2.21 eV and 1.90 eV. The decrease in optical band gap

energy was also observed by M. S. Hasan *et al.* to confirm the semiconducting nature of ferrites [36]. In addition, the alteration of cationic species (Mg and Co) in the lattice can influence charge transfer between ions. This charge transfer can affect the energy levels of electrons and holes within the material, leading to a change in the band gap.

3.7 Dielectric Properties

At 300 K, the dielectric constant (ϵ') of Mg²⁺ doped ZCL nano-ferrites versus frequency was measured within the 8 Hz to 8 MHz frequency range and the data are given in Fig. 12(a). The dielectric constant (ϵ') showed reducing trend with the increasing frequency and become constant at large frequency. Such trend is due to space charge polarization because of inhomogeneous structures of nanoparticles. This sort of nano ferrites dielectric behavior accredited to Maxwell-Wagner interfacial polarization in concurrence with Koop's phenomenological theory [70] in which the nano-ferrites act as a multilayer capacitor consisting of grains and grain boundaries. Moreover, the defects in nano-ferrites responsible for poor conductive grain boundaries in lower frequency, whereas in greater frequency, smooth grains are more effective due to high conductivity. The reduction in “ ϵ' ” values at high frequency is associated to interior grains because the charge carrier hopping do not follow the applied field [71]. In Mg²⁺ inserted ZCL nano-ferrites, the conduction sources including Fe³⁺—O²⁻—Me (Me is Mg²⁺, Zn²⁺, Co²⁺ and La³⁺) and Fe³⁺—O²⁻—Fe³⁺ are basis for hopping and it plays a significant role in the conduction mechanism.

At 300 K, the plot of dispersive loss ($\tan\delta$) and frequency is given in Fig. 12(b). The dispersive (tangent) loss demonstrates same trends for dielectric constant with an increasing frequency. At low frequency, the dispersive (tangent) loss has greater values for the as-prepared nano ferrites. It may be due to the crystal defects attributed to the domination of exceedingly resistive grain boundaries. At higher frequency dispersive (tangent) loss is larger due to low resistive grains [72]. The declination in both dielectric factors were also observed by Maria *et al.* in Mg doped Co-Zn ferrites [23].

3.8 VSM analysis

M-H loops for Mg²⁺ substituted ZCL nano-ferrites are shown in Fig. 13. The measured coercivity (H_c), remnant magnetization (M_r), saturation magnetization (M_s) and squareness ratio ($SQ = M_r/M_s$) from *M-H* loops are listed in Table 11. It can be seen that M_s decreases with the

addition of Mg^{2+} concentration which can be attributed to cations distributions. The addition of Mg^{2+} leads to a reduction in the saturation magnetization and remanence magnetization. In a ferromagnetic spinel structure, the magnetic ordering arises from super-exchange interactions between metal ions in the A and B sub-lattices. The decrease in saturation magnetization is attributed to the incorporation of iron into the A site giving rise to the diminishing strength of the exchange interaction between A and B sites. Furthermore, $CoFe_2O_4$ exhibits a mixed spinel structure featuring a non-collinear ferromagnetic spin arrangement, with crystallite sizes ranging from 20 to 10 nm. The reduction in saturation magnetization can also be attributed to the presence of this non-collinear spin configuration on the particle surfaces [73]. Also it may also attributed to the introduction Zn^{2+} in ZCL ferrites leads the decrease in A-B interactions and increase in B-B interactions [74]. In our work maximum M_s of 60.82 emu/g is observed which is higher than 42.29 mu/g found in Mg doped CoZn ferrites by Kaur *et al.* [75]. While, in current research work maximum $M_s = 60.82$ emu/g is observed. The coercivity (H_c) are ranging from 511 Oe to 1134 Oe and it decreases with the increase of Mg^{2+} concentration. M_r and M_S indicated the same behavior as coercivity (H_c). The squareness ratio indicates how square the hysteresis loop is [76]. Coercivity (H_c) is the magnetic field strength required to demagnetize the material. It is determined by examining the M-H loop during the decreasing field phase. As we reduce the applied field from its positive maximum, the magnetization will start decreasing. The coercivity is reached when the magnetization drops to zero or crosses a predefined threshold value in the negative direction. N. Tomas *et al.* also found the decrease in H_c in the range of 930 – 89 Oe with the addition of Mg^{2+} concentration [16]. In H_c is also decreasing with the increase of Mg^{2+} concentration as given in Table 11. H_c is associated to magnetocrystalline anisotropy and size of nanoparticles in ZCL ferrites. Hence, the reduction in values of H_c are attributed to magnetocrystalline anisotropy of ZCL ferrites due to the insertion of Mg^{2+} ions [69]. The decrease in anisotropy field is attributed to reduction in energy of domain walls [15].

The squareness ratio SQ decreased from 0.78 to 0.51 as concentration of Mg^{2+} increased from 0.0 to 0.6 and the calculated SQ being less than one, indicating the superparamagnetic behavior of Mg^{2+} substituted ZCL spinel ferrites [77]. Tulu Wegayehu Mammo *et al.* also investigated the reduction in magnetic parameters with increase of magnesium contents [15].

The anisotropy constant ($K = H_c \times M_s / 0.96$) and initial permeability ($\mu_i = M_s^2 \times D / K$) were also reported in Table 11. The addition of Mg^{2+} cations led to a decrease in the "K" value, and

the lowest initial permeability was observed at $x = 0.3$. Typically, "K" is impacted by crystallographic orientations, crystalline anisotropy, and particle size. When particle size increases "K" values decrease and domain walls are formed. In such instances, the dominant contribution to magnetization arises from the movement of domain walls rather than domain rotation. In the current research, the reduction in "K" values is ascribed to the presence of dopant ions [78].

Soft ferrites have significant microwave applications and the equation $\omega_m = 8\pi^2 M_s \gamma$ can be used to investigate the high-frequency (where, $\gamma = 2.8$ MHz/Oe is the gyromagnetic ratio) [26, 79]. Fig. 14 shows the response of " ω_m " for Mg^{2+} substituted ZCL nano ferrites from which it can be seen that the ferrites could be used for high-frequency strategies. At the same time, the current magnetic materials were capable to be functioned in microwave frequency range 13.4 – 5.7 GHz.

In order to justify the aspects of single domain (SD)/pseudo-single domain (PSD) and multi-domain (MD) behavior over RT, the field dependence of magnetization was measured and the data of dM/dH [80] which is identified as the magnetic susceptibility (χ) curve are shown in Fig. 15. For ideal domain ferrites consist of $M-H$ square curve where coercivity (H_C) is zero as $H \rightarrow 0$, $\chi = dM/dH$ has an important role. $\chi = dM/dH$ at $H \rightarrow 0$ with limited values verifying the features of SD/PSD and MD grains in synthesized Mg^{2+} doped ZCL ferrites as given in Table 11. Fig. 15 signifies the dM/dH against H curve specifying the peak at $\sim H_m$ and being split by $2H_m$ and symmetric about $H \rightarrow 0$. Table 11 shows the results at $H \rightarrow H_m$ of H_m and dM/dH . H_m has higher values than the H_C and it signifies the switching field distribution (SFD) due to disordered shell arrangements in PSD and MD grains [81]. At H_m the " χ " for peak heights are also illustrated in Table 11 and exposed the higher outcomes of " χ " at $H \rightarrow H_m$ than the values at $H \rightarrow 0$. At H_m the enhancement in both peak partitions and peak heights of " χ " leads to the stability and good crystallization cubic matrix of ferrites. While, the opposite behavior of peaks makes the nano-ferrites extremely unstable superparamagnetic domains [82].

Conclusion

Mg substituted $Zn_{0.4}Co_{0.6-x}Mg_xFe_{1.9}La_{0.1}O_4$ soft ferrites ($x = 0.00, 0.15, 0.30, 0.45, 0.60$) were prepared by co-precipitation route. The average crystallite size and lattice constant revealed reducing behavior for $x = 0.0 - 0.45$ with maximum value at $x = 0.60$. Different parameters were

calculated by the application of XRD data. The morphological analysis verified the agglomerated form of nanoparticles. Optical bandgap energy decreased from 2.61 eV to 1.47 eV and an additional optical band gap was also observed. DC electrical resistivity expressed opposed behavior in paramagnetic and ferromagnetic regions. The Curie temperature decreased with the growth of magnesium contents. Tetrahedral and octahedral bands were detected in the range of $550.96\text{ cm}^{-1} - 552.39\text{ cm}^{-1}$ and $413.57\text{ cm}^{-1} - 403.56\text{ cm}^{-1}$ respectively, in FTIR spectra. Five active phonon modes were identified ($\Gamma = 1A_{1g} + 1E_g + 3T_{2g}$) for regular spinel structure. Dielectric constant and dielectric loss exposed reducing trends with the increasing frequency. The magnetic parameters (M_r , M_s and H_c) declined with the addition of magnesium contents. The frequency range (13.4 – 5.7 GHz) was determined by using saturation magnetization and exposed that Mg^{2+} doped ZCL particles are favorite candidates for high-frequency devices.

Acknowledgement

The author Muhammad Imran Arshad is extremely grateful to HEC Pakistan for granting the opportunity of Postdoc under post doc batch 3. Ref: 3-1/PDFP/HEC/2022(B-3)/2320/02.

References

- [1] M. Hashim, S. Meena, R. Kotnala, S.E. Shirsath, P. Bhatt, S. Kumar, E. Şentürk, R. Kumar, N. Gupta, Exploring the structural, Mössbauer and dielectric properties of Co^{2+} incorporated $Mg_0.5Zn_{0.5-x}Co_xFe_2O_4$ nanocrystalline ferrite, *Journal of magnetism and magnetic materials*, 360 (2014) 21-33.
- [2] M. Abdellatif, A. Azab, M. Salerno, Effect of rare earth doping on the vibrational spectra of spinel Mn-Cr ferrite, *Materials Research Bulletin*, 97 (2018) 260-264.
- [3] R. Valenzuela, Novel applications of ferrites, *Physics Research International*, 2012 (2012).
- [4] K.K. Kefeni, T.A. Msagati, T.T. Nkambule, B.B.J.M.S. Mamba, E. C, Spinel ferrite nanoparticles and nanocomposites for biomedical applications and their toxicity, 107 (2020) 110314.
- [5] S. Zhang, X. Liu, L. Zhou, W.J.M.L. Peng, Magnetite nanostructures: one-pot synthesis, superparamagnetic property and application in magnetic resonance imaging, 68 (2012) 243-246.
- [6] M. Banerjee, A. Mukherjee, S. Chakrabarty, S. Basu, M.J.A.A.N.M. Pal, Bismuth-Doped Nickel Ferrite Nanoparticles for Room Temperature Memory Devices, 2 (2019) 7795-7802.
- [7] S. Goel, M. Bala, A. Garg, V. Shivling, S.J.M.T.P. Tyagi, Lanthanum doped barium hexaferrite nanoparticles for enhanced microwave absorption, (2020).
- [8] K. Mohit, V.R. Gupta, N. Gupta, S.J.C.I. Rout, Structural and microwave characterization of $Ni_{0.2}Co_xZn_{0.8-x}Fe_2O_4$ for antenna applications, 40 (2014) 1575-1586.
- [9] R. Jasrotia, V.P. Singh, B. Sharma, A. Verma, P. Puri, R. Sharma, M.J.J.o.A. Singh, Compounds, Sol-gel synthesized Ba-Nd-Cd-In nanohexaferrites for high frequency and microwave devices applications, (2020) 154687.

- [10] A. Nigam, S.J.C.I. Pawar, Structural, magnetic, and antimicrobial properties of zinc doped magnesium ferrite for drug delivery applications, 46 (2020) 4058-4064.
- [11] K. Srinivasamurthy, S. Kubrin, S. Matteppanavar, D. Sarychev, P.M. Kumar, H.W. Azale, B.J.C.I. Rudraswamy, Tuning of ferrimagnetic nature and hyperfine interaction of Ni²⁺ doped cobalt ferrite nanoparticles for power transformer applications, 44 (2018) 9194-9203.
- [12] K. Ukoba, A. Eloka-Eboka, F. Inambao, Review of nanostructured NiO thin film deposition using the spray pyrolysis technique, Renewable and Sustainable Energy Reviews, 82 (2018) 2900-2915.
- [13] S. Giri, S. Samanta, S. Maji, S. Ganguli, A. Bhaumik, Magnetic properties of α -Fe₂O₃ nanoparticle synthesized by a new hydrothermal method, Journal of Magnetism and Magnetic Materials, 285 (2005) 296-302.
- [14] P. Singjai, K. Wongwigkarn, Y. Laosiritaworn, R. Yimnirun, S. Maensiri, Carbon encapsulated nickel nanoparticles synthesized by a modified alcohol catalytic chemical vapor deposition method, Current Applied Physics, 7 (2007) 662-666.
- [15] T.W. Mammo, N. Murali, Y.M. Sileshi, T. Arunamani, Studies of structural, morphological, electrical, and magnetic properties of Mg-substituted Co-ferrite materials synthesized using sol-gel autocombustion method, Physica B: Condensed Matter, 523 (2017) 24-30.
- [16] N. Thomas, P. Jithin, V. Sudheesh, V. Sebastian, Magnetic and dielectric properties of magnesium substituted cobalt ferrite samples synthesized via one step calcination free solution combustion method, Ceramics International, 43 (2017) 7305-7310.
- [17] M. Hasan, M. Arshad, A. Ali, K. Mahmood, N. Amin, S. Ali, M. Khan, G. Mustafa, M. Khan, M. Saleem, Mg and La co-doped ZnNi spinel ferrites for low resistive applications, Materials Research Express, 6 (2018) 016302.
- [18] N. Amin, R. Bilal, G. Mustafa, A. Aslam, M. Hasan, K. Hussain, M. Tabassum, M. Fatima, Z. Khan, A. Naseem, IMPACTS OF SUBSTITUTING Ni²⁺ IONS ON STRUCTURAL AND ELECTRICAL PROPERTIES OF W-TYPE BARIUM BASED HEXAFERRITES, DIGEST JOURNAL OF NANOMATERIALS AND BIOSTRUCTURES, 14 (2019) 501-507.
- [19] T. Dippong, E.A. Levei, G. Borodi, F. Goga, L. Barbu Tudoran, Influence of Co/Fe ratio on the oxide phases in nanoparticles of Co_xFe_{3-x}O₄, Journal of Thermal Analysis and Calorimetry, 119 (2015) 1001-1009.
- [20] T. Dippong, E.A. Levei, O. Cadar, Investigation of structural, morphological and magnetic properties of MFe₂O₄ (M= Co, Ni, Zn, Cu, Mn) obtained by thermal decomposition, International Journal of Molecular Sciences, 23 (2022) 8483.
- [21] T. Dippong, E.A. Levei, O. Cadar, I.G. Deac, M. Lazar, G. Borodi, I. Petean, Effect of amorphous SiO₂ matrix on structural and magnetic properties of Cu_{0.6}Co_{0.4}Fe₂O₄/SiO₂ nanocomposites, Journal of Alloys and Compounds, 849 (2020) 156695.
- [22] S. Bhukal, R. Sharma, S. Mor, S. Singhal, Mg-Co-Zn magnetic nanoferrites: characterization and their use for remediation of textile wastewater, Superlattices and Microstructures, 77 (2015) 134-151.
- [23] M.Y. Lodhi, K. Mahmood, A. Mahmood, H. Malik, M.F. Warsi, I. Shakir, M. Asghar, M.A. Khan, New Mg_{0.5}Co_xZn_{0.5-x}Fe₂O₄ nano-ferrites: structural elucidation and electromagnetic behavior evaluation, Current Applied Physics, 14 (2014) 716-720.
- [24] M.A. Rafiq, M.A. Khan, M. Asghar, S. Ilyas, I. Shakir, M. Shahid, M.F. Warsi, Influence of Co²⁺ on structural and electromagnetic properties of Mg-Zn nanocrystals synthesized via co-precipitation route, Ceramics International, 41 (2015) 10501-10505.

- [25] Y. Liu, S. Wei, Y. Wang, H. Tian, H. Tong, B. Xu, Characterization of (Mg, La) Substituted Ni-Zn Spinel Ferrite, *Physics Procedia*, 50 (2013) 43-47.
- [26] S. Gaba, A. Kumar, P.S. Rana, M. Arora, Influence of La³⁺ ion doping on physical properties of magnesium nanoferrites for microwave absorption application, *Journal of Magnetism and Magnetic Materials*, 460 (2018) 69-77.
- [27] T. Dippong, E.A. Levei, O. Cadar, A. Mesaros, G. Borodi, Sol-gel synthesis of CoFe₂O₄:SiO₂ nanocomposites—insights into the thermal decomposition process of precursors, *Journal of analytical and applied pyrolysis*, 125 (2017) 169-177.
- [28] P. Barvinschi, O. Stefanescu, T. Dippong, S. Sorescu, M. Stefanescu, CoFe₂O₄/SiO₂ nanocomposites by thermal decomposition of some complex combinations embedded in hybrid silica gels, *Journal of thermal analysis and calorimetry*, 112 (2013) 447-453.
- [29] T. Dippong, E.-A. Levei, D. Toloman, L. Barbu-Tudoran, O. Cadar, Investigation on the formation, structural and photocatalytic properties of mixed Mn-Zn ferrites nanoparticles embedded in SiO₂ matrix, *Journal of Analytical and Applied Pyrolysis*, 158 (2021) 105281.
- [30] M. Bhandare, H. Jamadar, A. Pathan, B. Chougule, A.J.J.o.a. Shaikh, compounds, Dielectric properties of Cu substituted Ni_{0.5-x}Zn_{0.3}Mg_{0.2}Fe₂O₄ ferrites, 509 (2011) L113-L118.
- [31] R.R. Kanna, N. Lenin, K. Sakthipandi, M.J.C.I. Sivabharathy, Impact of lanthanum on structural, optical, dielectric and magnetic properties of Mn_{1-x}Cu_xFe_{1.85}La_{0.15}O₄ spinel nanoferrites, 43 (2017) 15868-15879.
- [32] M.A. Maksoud, A. El-Ghandour, A. Ashour, M. Atta, S. Abdelhaleem, A.H. El-Hanbaly, R.A. Fahim, S.M. Kassem, M. Shalaby, A.J.J.o.R.E. Awed, La³⁺ doped LiCo_{0.25}Zn_{0.25}Fe₂O₄ spinel ferrite nanocrystals: insights on structural, optical, and magnetic properties, (2020).
- [33] M. Hasan, S. Ali, M. Rizwan, M. Khan, H.N. Ullah, M.I. Irfan, Structural, Optical, Electrical and Magnetic Properties of Cu_{0.2}Zn_{0.2}Ni_{0.6-2x}Mg_xFe₂O₄ (x= 0.00, 0.15, 0.30, 0.45, 0.60) Soft Ferrites, *Journal of Alloys and Compounds*, (2023) 170392.
- [34] M. Nabi, M. Moin, M. Hasan, M. Arshad, A. Bibi, N. Amin, K. Mahmood, S. Ali, Study of electrical Transport properties of cadmium-doped Zn–Mn soft ferrites by Co-precipitation method, *Journal of Superconductivity and Novel Magnetism*, 34 (2021) 1813-1822.
- [35] S. Anand, A.P. Amaliya, M.A. Janifer, S.J.M.E.M. Pauline, Structural, morphological and dielectric studies of zirconium substituted CoFe₂O₄ nanoparticles, 3 (2017) 168-173.
- [36] M. Hasan, S. Ali, M. Khan, M. Rizwan, M. Zulqarnain, A. Hussain, Structural, optical, electrical and magnetic tuning based on Zn substitution at A site in yttrium doped spinel ferrites, *Materials Chemistry and Physics*, 301 (2023) 127538.
- [37] W.A. Farooq, M. Sajjad Ul Hasan, M.I. Khan, A.R. Ashraf, M. Abdul Qayyum, N. Yaqub, M.A. Almutairi, M. Atif, A. Hanif, Structural, Optical and Electrical Properties of Cu_{0.6}CoxZn_{0.4-x}Fe₂O₄ (x= 0.0, 0.1, 0.2, 0.3, 0.4) Soft Ferrites, *Molecules*, 26 (2021) 1399.
- [38] M. Akhtar, M. Hasan, N. Amin, N. Morley, M.I. Arshad, Tuning structural, electrical, dielectric and magnetic properties of Mg–Cu–Co ferrites via dysprosium (Dy³⁺) doping, *Journal of Rare Earths*, (2023).
- [39] N. Amin, M.S.U. Hasan, Z. Majeed, Z. Latif, M.A. un Nabi, K. Mahmood, A. Ali, K. Mehmood, M. Fatima, M.J.C.I. Akhtar, Structural, electrical, optical and dielectric properties of yttrium substituted cadmium ferrites prepared by Co-Precipitation method, (2020).
- [40] M. Khan, G. Hassan, M. Hasan, S.A. Abubshait, H.A. Abubshait, W. Al-Masry, Q. Mahmood, A. Mahmood, S.M. Ramay, Investigations on the efficiency variation of zinc and

gallium Co-doped TiO₂ based dye sensitized solar cells, *Ceramics International*, 46 (2020) 24844-24849.

[41] A. Mujtaba, M. Khan, M. Hasan, S. Ali, W. Shahid, M. Fatima, H.S. Abd-Rabboh, N. Alwadai, Tailoring the structural, optical, photoluminescence, dielectric and electrical properties of Zn_{0.6}Ni_{0.2}Mg_{0.2}Fe_{2-x}LaxO₄ (x= 0.00, 0.0125, 0.0250, 0.0375), *Journal of Materials Research and Technology*, 23 (2023) 4538-4550.

[42] V. Chaudhari, S.E. Shirsath, M. Mane, R. Kadam, S. Shelke, D. Mane, Crystallographic, magnetic and electrical properties of Ni_{0.5}Cu_{0.25}Zn_{0.25}LaxFe_{2-x}O₄ nanoparticles fabricated by sol-gel method, *Journal of alloys and compounds*, 549 (2013) 213-220.

[43] M. Saqib, S. Ali, M. Zulqarnain, M.U. Qadri, M. Riaz, M. Hasan, M. Khan, M. Tahir, M. Arshad, H. Rani, Temperature-dependent variations in structural, magnetic, and optical behavior of doped ferrites nanoparticles, *Journal of Superconductivity and Novel Magnetism*, 34 (2021) 609-616.

[44] M.N. Akhtar, M.A. Khan, Effect of rare earth doping on the structural and magnetic features of nanocrystalline spinel ferrites prepared via sol gel route, *Journal of Magnetism and Magnetic Materials*, 460 (2018) 268-277.

[45] I. Ahmad, T. Abbas, M. Islam, A. Maqsood, Study of cation distribution for Cu-Co nanoferrites synthesized by the sol-gel method, *Ceramics International*, 39 (2013) 6735-6741.

[46] K.M. Batoo, G. Kumar, Y. Yang, Y. Al-Douri, M. Singh, R.B. Jotania, A. Imran, Structural, morphological and electrical properties of Cd²⁺ doped MgFe_{2-x}O₄ ferrite nanoparticles, *Journal of Alloys and Compounds*, 726 (2017) 179-186.

[47] M. Zulqarnain, S. Ali, U. Hira, J. Feng, M. Khan, M. Rizwan, K. Javed, G. Farid, M. Hasan, Superparamagnetic contributions, optical band gap tuning and dominant interfacial resistive mechanisms in ferrites nanostructures, *Journal of Alloys and Compounds*, 894 (2022) 162431.

[48] A. Goldman, *Modern ferrite technology*, Springer Science & Business Media, 2006.

[49] R. Sharma, S. Singhal, Structural, magnetic and electrical properties of zinc doped nickel ferrite and their application in photo catalytic degradation of methylene blue, *Physica B: Condensed Matter*, 414 (2013) 83-90.

[50] R. Sharma, P. Thakur, P. Sharma, V. Sharma, Ferrimagnetic Ni²⁺ doped Mg-Zn spinel ferrite nanoparticles for high density information storage, *Journal of Alloys and Compounds*, 704 (2017) 7-17.

[51] P. Thakur, R. Sharma, M. Kumar, S. Katyal, N. Negi, N. Thakur, V. Sharma, P. Sharma, Superparamagnetic La doped Mn-Zn nano ferrites: dependence on dopant content and crystallite size, *Materials Research Express*, 3 (2016) 075001.

[52] M. Khan, M. Waqas, M. Naeem, M. Hasan, M. Iqbal, A. Mahmood, S.M. Ramay, W. Al-Masry, S.A. Abubshait, H.A. Abubshait, Magnetic behavior of Ga doped yttrium iron garnet ferrite thin films deposited by sol-gel technique, *Ceramics International*, 46 (2020) 27318-27325.

[53] M. NABI, M. Sharif, G. Mustafa, A. ALIa, K. Mahmood, N. ALIc, N. Amin, M. Ahmad, N. Sabir, M. Asif, STRUCTURAL AND THERMOELECTRIC POWER STUDIES OF Sm³⁺-SUBSTITUTED Li-Ni-SPINEL FERRITE, *DIGEST JOURNAL OF NANOMATERIALS AND BIOSTRUCTURES*, 13 (2018) 1111-1116.

[54] M. Hasan, M. Khan, S. Kanwal, M. Irfan, T.I. Al-Muhimeed, S. Mumtaz, Structural, optical and electrical impacts of Ni²⁺ on Mg_{1-x}Fe_{1.9}Sm_{0.1}O₄ (x= 0.0, 0.2, 0.4 and 0.6) spinel ferrites, *Digest Journal of Nanomaterials & Biostructures (DJNB)*, 17 (2022).

- [55] S. Yasmeen, F. Iqbal, T. Munawar, M.A. Nawaz, M. Asghar, A.J.C.I. Hussain, Synthesis, structural and optical analysis of surfactant assisted ZnO–NiO nanocomposites prepared by homogeneous precipitation method, 45 (2019) 17859-17873.
- [56] M.M.L. Sonia, S. Anand, V.M. Vinoseel, M.A. Janifer, S.J.J.o.M.S.M.i.E. Pauline, Effect of lattice strain on structural, magnetic and dielectric properties of sol–gel synthesized nanocrystalline Ce³⁺ substituted nickel ferrite, 29 (2018) 15006-15021.
- [57] R. Gupta, A. Sood, P. Metcalf, J. Honig, Raman study of stoichiometric and Zn-doped Fe₃O₄, Physical Review B, 65 (2002) 104430.
- [58] M.A.U. Nabi, M. Moin, M. Hasan, M. Arshad, A. Bibi, N. Amin, K. Mahmood, S. Ali, Study of electrical transport properties of cadmium-doped Zn–Mn soft ferrites by co-precipitation method, Journal of Superconductivity and Novel Magnetism, 34 (2021) 1813-1822.
- [59] R. Waldron, Infrared spectra of ferrites, Physical review, 99 (1955) 1727.
- [60] P. Graves, C. Johnston, J. Campaniello, Raman scattering in spinel structure ferrites, Materials Research Bulletin, 23 (1988) 1651-1660.
- [61] M. Popa, J. Frantti, M. Kakihana, Lanthanum ferrite LaFeO₃+ d nanopowders obtained by the polymerizable complex method, Solid State Ionics, 154 (2002) 437-445.
- [62] M.I. Arshad, M. Hasan, A.U. Rehman, M. Akhtar, N. Amin, K. Mahmood, A. Ali, T. Trakoolwilaiwan, N.T.K. Thanh, Structural, optical, electrical, dielectric, molecular vibrational and magnetic properties of La³⁺ doped Mg–Cd–Cu ferrites prepared by Co-precipitation technique, Ceramics International, 48 (2022) 14246-14260.
- [63] M. Abdellatif, G. Abdelrasoul, M. Salerno, I. Liakos, A. Scarpellini, S. Marras, A. Diaspro, Fractal analysis of inter-particle interaction forces in gold nanoparticle aggregates, Colloids and Surfaces A: Physicochemical and Engineering Aspects, 497 (2016) 225-232.
- [64] M. Raghasudha, D. Ravinder, P. Veerasomaiah, Electrical resistivity studies of Cr doped Mg nano-ferrites, Materials Discovery, 2 (2015) 50-54.
- [65] R.G. Kharabe, R.S. Devan, B.K. Chougale, Structural and electrical properties of Cd-substituted Li–Ni ferrites, Journal of Alloys and Compounds, 463 (2008) 67-72.
- [66] K. Jalaiah, K.C. Mouli, R. Krishnaiah, K.V. Babu, P.S. Rao, The structural, DC resistivity and magnetic properties of Zr and Co co-substituted Ni_{0.5}Zn_{0.5}Fe₂O₄, Heliyon, 5 (2019) e01800.
- [67] A. Manikandan, L.J. Kennedy, M. Bououdina, J.J. Vijaya, Synthesis, optical and magnetic properties of pure and Co-doped ZnFe₂O₄ nanoparticles by microwave combustion method, Journal of magnetism and magnetic materials, 349 (2014) 249-258.
- [68] K. Hussain, N. Amin, M. Ajaz-Un-Nabi, A. Ali, K. Mahmood, G. Mustafa, M. Sharif, M. Hasan, N. Sabir, S. Ali, Investigation of structural and electrical properties of Ce³⁺ ions substituted Cd-Co Ferrites, Dig. J. Nanomater. Biostruct., 14 (2019) 85-92.
- [69] A.G. Abraham, A. Manikandan, E. Manikandan, S. Vadivel, S. Jaganathan, A. Baykal, P.S. Renganathan, Enhanced magneto-optical and photo-catalytic properties of transition metal cobalt (Co²⁺ ions) doped spinel MgFe₂O₄ ferrite nanocomposites, Journal of Magnetism and Magnetic Materials, 452 (2018) 380-388.
- [70] J.C. Maxwell, Electricity and magnetism, , Dover, New York,, (1954).
- [71] Z. Ahmad, S. Atiq, S.K. Abbas, S.M. Ramay, S. Riaz, S.J.C.I. Naseem, Structural and complex impedance spectroscopic studies of Mg-substituted CoFe₂O₄, 42 (2016) 18271-18282.
- [72] E. Melagiriyyappa, H. Jayanna, B. Chougule, Dielectric behavior and ac electrical conductivity study of Sm³⁺ substituted Mg–Zn ferrites, Materials chemistry and physics, 112 (2008) 68-73.

- [73] H. Moradmard, S.F. Shayesteh, P. Tohidi, Z. Abbas, M. Khaleghi, Structural, magnetic and dielectric properties of magnesium doped nickel ferrite nanoparticles, *Journal of Alloys and Compounds*, 650 (2015) 116-122.
- [74] T. Dippong, I.G. Deac, O. Cadar, E.A. Levei, Effect of silica embedding on the structure, morphology and magnetic behavior of $(\text{Zn}_{0.6}\text{Mn}_{0.4}\text{Fe}_2\text{O}_4)_\delta/(\text{SiO}_2)_{(100-\delta)}$ nanoparticles, *Nanomaterials*, 11 (2021) 2232.
- [75] M. Kaur, P. Jain, M. Singh, Studies on structural and magnetic properties of ternary cobalt magnesium zinc (CMZ) $\text{Co}_{0.6-x}\text{Mg}_x\text{Zn}_{0.4}\text{Fe}_2\text{O}_4$ ($x = 0.0, 0.2, 0.4, 0.6$) ferrite nanoparticles, *Materials Chemistry and Physics*, 162 (2015) 332-339.
- [76] T. Dippong, E.A. Levei, I.G. Deac, I. Petean, O. Cadar, Dependence of structural, morphological and magnetic properties of manganese ferrite on Ni-Mn substitution, *International Journal of Molecular Sciences*, 23 (2022) 3097.
- [77] M.N. Akhtar, M.S. Nazir, Z. Tahir, S. Qamar, M.A.J.C.I. Khan, Impact of Co doping on physical, structural, microstructural and magnetic features of MgZn nanoferrites for high frequency applications, 46 (2020) 1750-1759.
- [78] T. Dippong, E.A. Levei, C. Leostean, O. Cadar, Impact of annealing temperature and ferrite content embedded in SiO_2 matrix on the structure, morphology and magnetic characteristics of $(\text{Co}_{0.4}\text{Mn}_{0.6}\text{Fe}_2\text{O}_4)_\delta (\text{SiO}_2)_{100-\delta}$ nanocomposites, *Journal of Alloys and Compounds*, 868 (2021) 159203.
- [79] A. Majeed, M.A. Khan, F. ur Raheem, A. Hussain, F. Iqbal, G. Murtaza, M.N. Akhtar, I. Shakir, M.F. Warsi, Structural elucidation and magnetic behavior evaluation of rare earth (La, Nd, Gd, Tb, Dy) doped BaCoNi-X hexagonal nano-sized ferrites, *Journal of magnetism and magnetic materials*, 408 (2016) 147-151.
- [80] I.P. Muthuselvam, R.J.S.S.S. Bhowmik, Structural phase stability and magnetism in Co_2FeO_4 spinel oxide, 11 (2009) 719-725.
- [81] W. Zhang, A. Sun, X. Zhao, N. Suo, L. Yu, Z.J.J.o.S.-G.S. Zuo, Technology, Structural and magnetic properties of La^{3+} ion doped Ni-Cu-Co nano ferrites prepared by sol-gel auto-combustion method, 90 (2019) 599-610.
- [82] I.P. Muthuselvam, R.J.J.o.M. Bhowmik, M. Materials, Mechanical alloyed Ho^{3+} doping in CoFe_2O_4 spinel ferrite and understanding of magnetic nanodomains, 322 (2010) 767-776.